# Chapter 9

# Computational Study on the Effect of Controlled Stereochemistry on Oxygen Permeability in EVOH Materials

This work was done as a collaborative effort with Dr. Valeria Molinero in the Goddard group at Caltech.

## 9.1 Abstract

The purpose of this research is to explore the microscopic structure and dynamics of two ethylene vinyl alcohol (EVOH) copolymers differing only in the relative stereochemistry between neighboring 1,2-diols by means of molecular dynamics simulations. The spatial distribution of hydroxyl groups, their hydrogen bonding pattern, and free volume distribution were analyzed in an attempt to explain the different properties experimentally observed for these two materials which were detailed in Chapter 8. As expected, the local topology of the 1,2-diols indeed effects the global three-dimensional polymer structures, as characterized by their hydrogen bond networks.

## 9.2 Introduction

Ethylene vinyl alcohol (EVOH) copolymers possess excellent barrier properties, especially towards oxygen gas diffusion.[1, 2] They have therefore found many commercial applications in the food packaging as well as in the biomedical industries.[1, 3, 4] Until recently, regioregular and stereoregular EVOH materials could not be synthesized. Rather, these copolymers were made through the free-radical copolymerization of vinyl acetate and ethylene, which resulted in varying amounts of uncontrolled branching. Through the use of ring-opening metathesis polymerization (ROMP) with functional group tolerant late transition metal ruthenium olefin metathesis catalysts, regio- and stereo-regular EVOH materials can now be synthesized as illustrated in Scheme 9.1.[4][*]

It was evident from experimental results that a difference in stereochemistry between neighboring alcohol functionalites in EVOH have a dramatic effect on the structure of the copolymer both in solution as well as in the solid state.[5] In order to gain a better insight into the role that stereochemistry plays in the material morphology and performance, a detailed set of molecular dynamic simulations was undertaken.

---

[*] See Chapter 8.

**Scheme 9.1**: General sythetic route to syn-(polymer **5**) and anti-diols (polymer **6**) along EVOH backbone from the *trans*- and *cis*-acetonide monomers **1** and **2**, respectively.

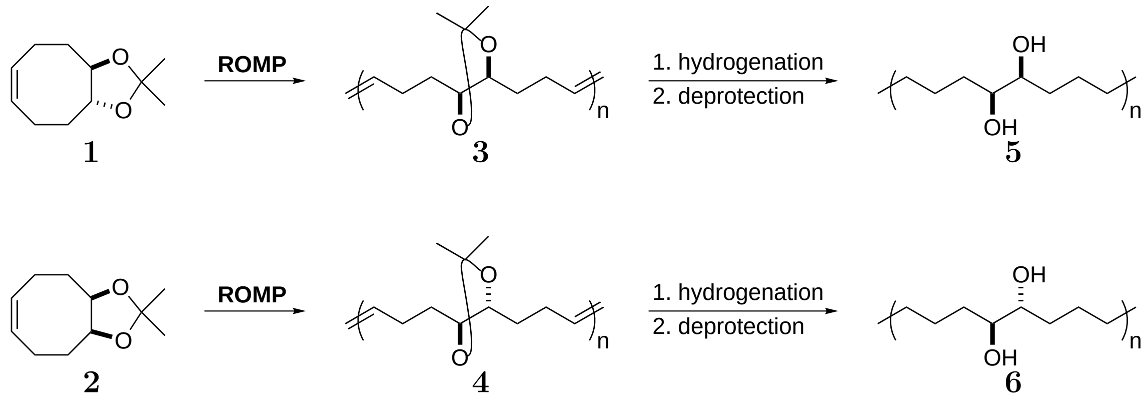

## 9.3 Simulation Methods

The initial sample EVOH structures of **5** and **6** were made using the Amorphous Builder of Cerius2,[6] which uses Monte Carlo techniques to build an amorphous structure with a three dimensional periodic cell. This Monte Carlo build was followed with an extensive series of annealing simulations in which the volume and temperature were varied systematically to achieve a fully equilibrated system at the target temperature and pressure. Each simulated system consists of four wholly syn or anti EVOH 20-mer chains (total number of atoms in the system is 2088). Three independent samples were constructed for both polymers **5** and **6**.

The annealing procedure for constructing the amorphous structure is as follows. Since the experimental data indicates that the density is 1.09 g/cm$^3$ at 300 K for EVOH polymer **5**, the initial polymer structure was prepared using a supercell appropriate for a density of 1.1 g/cm$^3$. Monte Carlo techniques were employed to construct initial configurations at 60% of the target density (1.1 g/cm$^3$) which were then relaxed by applying the following annealing procedure: First, the structure was gradually expanded by 50% of its initial volume over a period of 50 ps while the temperature was simultaneously increased from 300 K to 700 K. Next, NVT molecular dynamics (MD) simulations were performed at 700 K with the expanded volume for 50 ps. Next, the structure was compressed back to the initial volume over 50 ps while cooling the temperature to the target temperature of 300 K. This process was repeated five times. Then, at the final target density (1.1 g/cm$^3$), 100 ps of NVT MD (fixed volume and Nose-Hoover thermostat[7–10] at 300 K) was carried out. This was followed by a step-wise increase of the temperature to 430 K where an NVT simulation for 100 ps followed by an NPT simulation for 400 ps to relax the density of the system were carried out. This was followed by a continuous cooling ramp of temperature from 430 to 300 K over a 520 ps timescale at constant pressure (1 atm). The annealing simulations were performed with LAMMPS (Large-scale Atomic/Molecular Massively Parallel Simulator) code from Plimpton at Sandia (modified to handle our force fields).[11, 12] The equations of motion were integrated using the Verlet algorithm[13] with a time step of 1.0 fs, and the Particle-Particle Particle-Mesh (PPPM) method[14] was used for the electrostatic interactions.

After annealing the structures as described above, NPT MD simulations were performed with the LAMMPS code at 300 K for 1 ns. This led to a final density of 1.03 g/cm$^3$ ± 0.02 g/cm$^3$ for both **5** and **6** polymers at 300 K which compares well with the experimental value of 1.09 g/cm$^3$ for **5**.

To describe inter- and intra-molecular interactions, the OPLS-AA force field was employed.[15–18] The standard geometric combination rules for the cross van der Waals interactions were used and the total potential energy is given as follows:

$$\mathrm{E_{total}} = \mathrm{E_{vdW}} + \mathrm{E_Q} + \mathrm{E_{bond}} + \mathrm{E_{angle}} + \mathrm{E_{torsion}}$$

where $\mathrm{E_{total}}$, $\mathrm{E_{vdW}}$, $\mathrm{E_Q}$, $\mathrm{E_{bond}}$, $\mathrm{E_{angle}}$, and $\mathrm{E_{torsion}}$ are the total energies and the van der Waals, electrostatic, bond stretching, angle bending, and torsion components, respectively.

## 9.4 Results and Discussion

### 9.4.1 Hydrogen Bond Analysis

An attempt was made to identify the glass transition temperature, $T_g$, for both **5** and **6** by analyzing plots of energy vs temperature and volume vs temperature of the cooling ramps described above. Unfortunately, no significant change in slope was observed in either system. However, a drastic change in atom mobility as a function of temperature was noted. At 430 K, both systems possessed liquid-like mobilities while at 300 K, the atom displacement was $< 2$ Å for 500 ps as seen in Figure 9.1. This suggests that both polymers are in the glassy state at 300 K in agreement with the experimentally determined $T_g$ of 34.5 and 50 °C for **5** and **6**, respectively. This conclusion is based on the low value of the atom mobilities and the appearance of a plateau evident in Figure 9.1. It is worth noting that the mobility of the hydroxyl group (O) is higher than that of the polymer backbone (C) atoms suggesting that if any hydrogen bonding exists, it does not impose a constraint on the -OH librations.

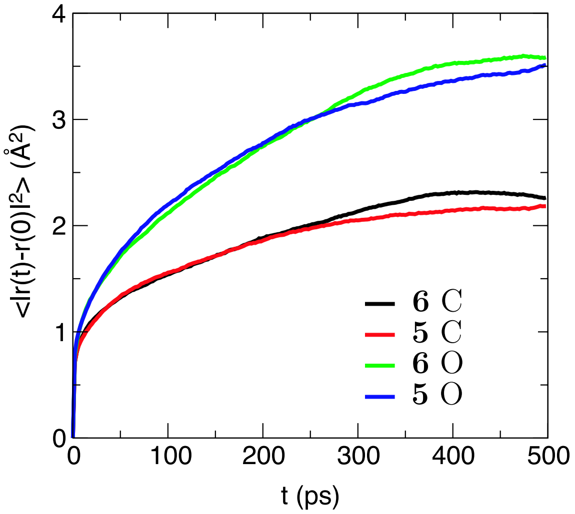

**Figure 9.1**: Mean square displacement of carbon and oxygen atoms in both syn diol polymer **5** and anti diol polymer **6** at 300 K.

The local topology of the neighboring 1,2-diols is quite different for EVOH polymers **5** and **6**. The formation of 1,2-hydrogen bond interaction between the syn diols in **5** is prevalent as seen in Figure 9.2. On the other hand, 1,2-hydrogen bonds are not observed for the anti diols in **6** (Figure 9.2). In order to form a neighboring intramolecular hydrogen bond in **6** it is necessary to greatly alter the polymer conformation. The structure resulting from this conformational change is likely to have an unfavorable effect on packing of the polymer chains. Furthermore, in no case are any hydrogen bonding interactions between adjacent neighboring pairs observed. The correlation of intra-chain hydrogen bonds is short ranged and micelle-like structures with segregated hydroxyl domains are not observed.

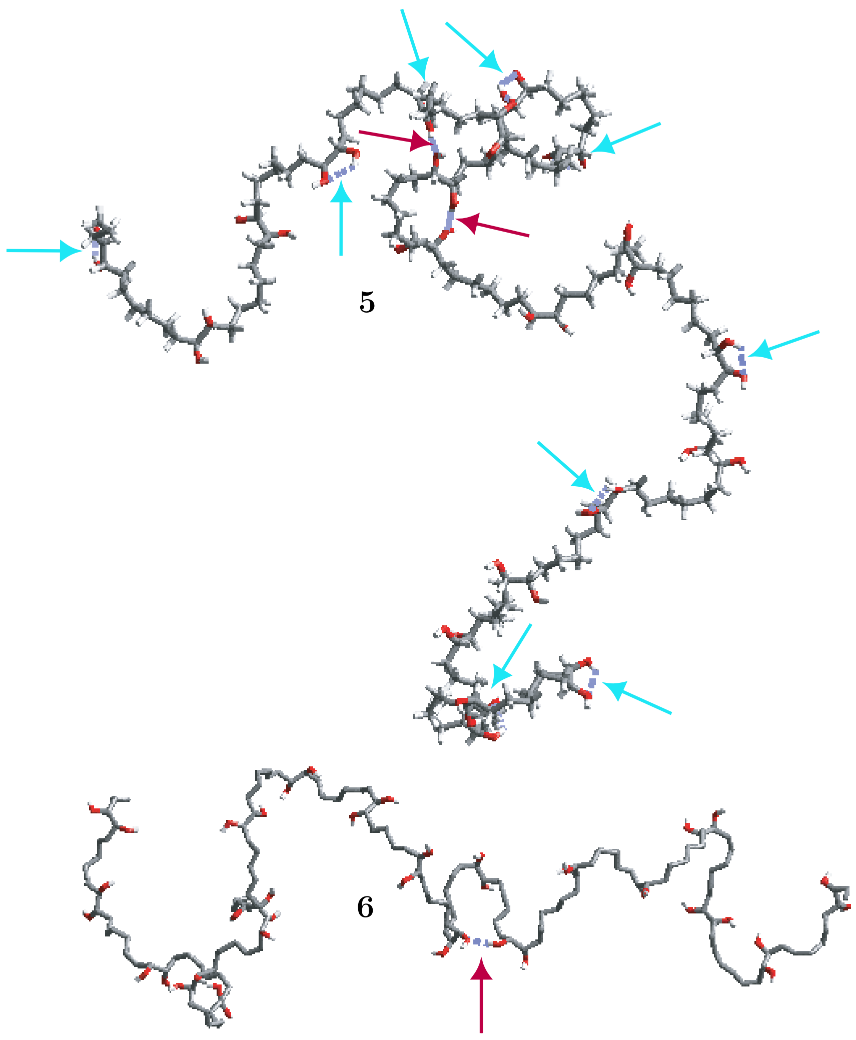

**Figure 9.2**: Types of intra-chain hydrogen bonding in both **5** and **6**. The blue arrows indicate the presence of neighboring 1,2-diol intramolecular hydrogen bonds and the red arrows point to non-neighboring intramolecular hydrogen bonds.

In an attempt to further characterize the hydrogen bond (H-bond) patterns in the systems, the three-dimensional H-bonding networks in both polymers and computed the distribution of H-bonding clusters were analyzed. The hydrogen bond connectivity was defined using a geometric criterion. A hydrogen bond was considered to be formed if the donor hydrogen and acceptor oxygen were less than 2.5 Å apart. If at least one hydrogen bond exists between two hydroxyl groups, they were assumed to belong to the same cluster. Figure 9.3 shows the hydrogen bond networks for typical configurations of polymers **6** and **5**.

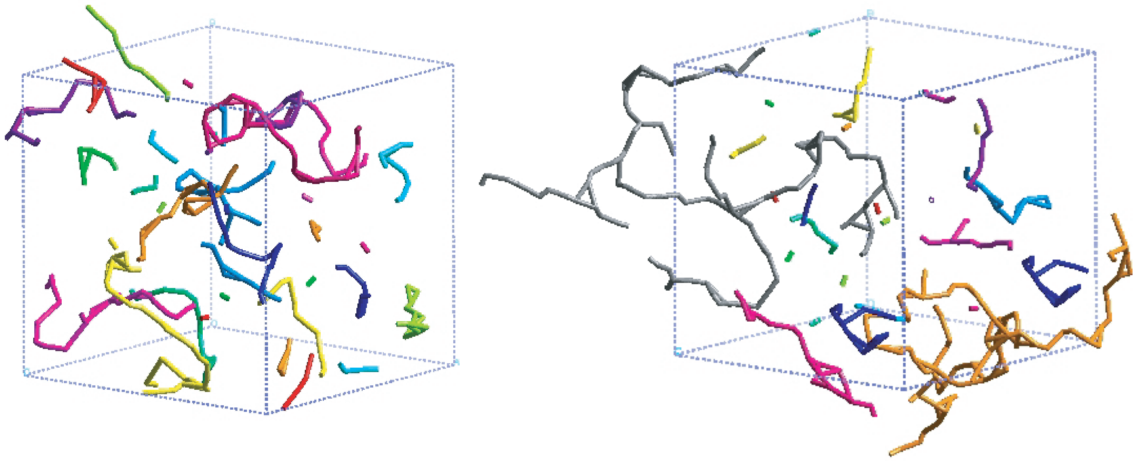

anti diols (**6**) syn diols (**5**)

**Figure 9.3**: 3-D representation of extended hydrogen bonding in EVOH.

Both polymers form mainly one-dimensional clusters. This is expected as each hydroxyl group has only one hydrogen bond donor and acceptor. However, the syn relationship of the diols in polymer **5** displays a characteristically longer connectivity than is observed in **6**. The average length of the hydrogen bond clusters were quantified and differ by more than 50%: the average number of hydroxyl groups in the cluster is 4.0 and 6.6 for anti and syn polymers, respectively. Moreover, the difference in the distribution of the cluster sizes for the two polymers as shown by the graph in Figure 9.4 is striking. The probability of finding clusters with > 20 hydroxyl groups is zero for the anti polymer **6**. Conversely, syn polymer **5** possesses a broad distribution of cluster sizes. These distribution are in agreement with the qualitative view

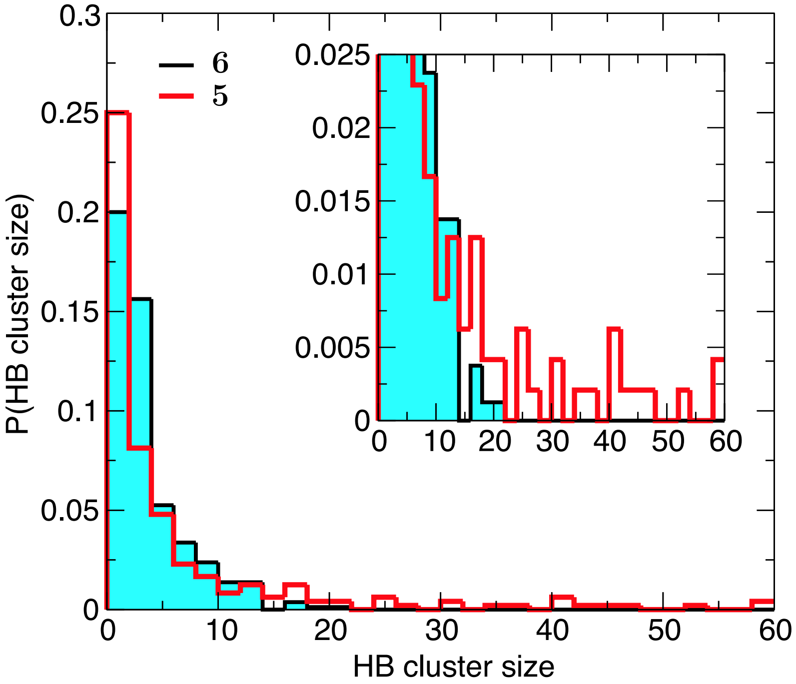

**Figure 9.4**: Probability of hydrogen bond cluster sizes.

illustrated by the Figure 9.3.

### 9.4.2 Free Volume Analysis

The free volume (FV) for the two polymers were computed. The FV is defined as the volume fraction of the total volume available for the probe. The FV accessible to a probe of radius $R_p$ was calculated over a three-dimensional grid of size 0.1 Å, and measuring the space occupied by spheres of radius $R_a + R_p$, where $R_a$ is the contact radius (1.2, 1.52, and 1.70 Å for H, O, and C, respectively). The void percolation radius $R_{pc}$ is defined as the largest probe that senses accessible FV channels percolated in all directions. A channel is percolated if it is connected with its periodic images in the three cartesian directions. In a percolated structure, the ratio between the volume of the largest (percolated) void and any other void is very big. This is illustrated in Figure 9.5 which shows the FV fraction largest and second largest voids for both polymers equilibrated at 300 K. The arrow in Figure 9.5 indicates a percolating probe radius, $R_{pc}$, which is approximately 0.6 Å. The $R_{pc}$ is smaller than any molecular solute such as oxygen or water; it is close to the 0.55 Å for a glass of random close-packed spheres and well below the 0.9–1.1 Å computed for atactic polypropylene.[19]

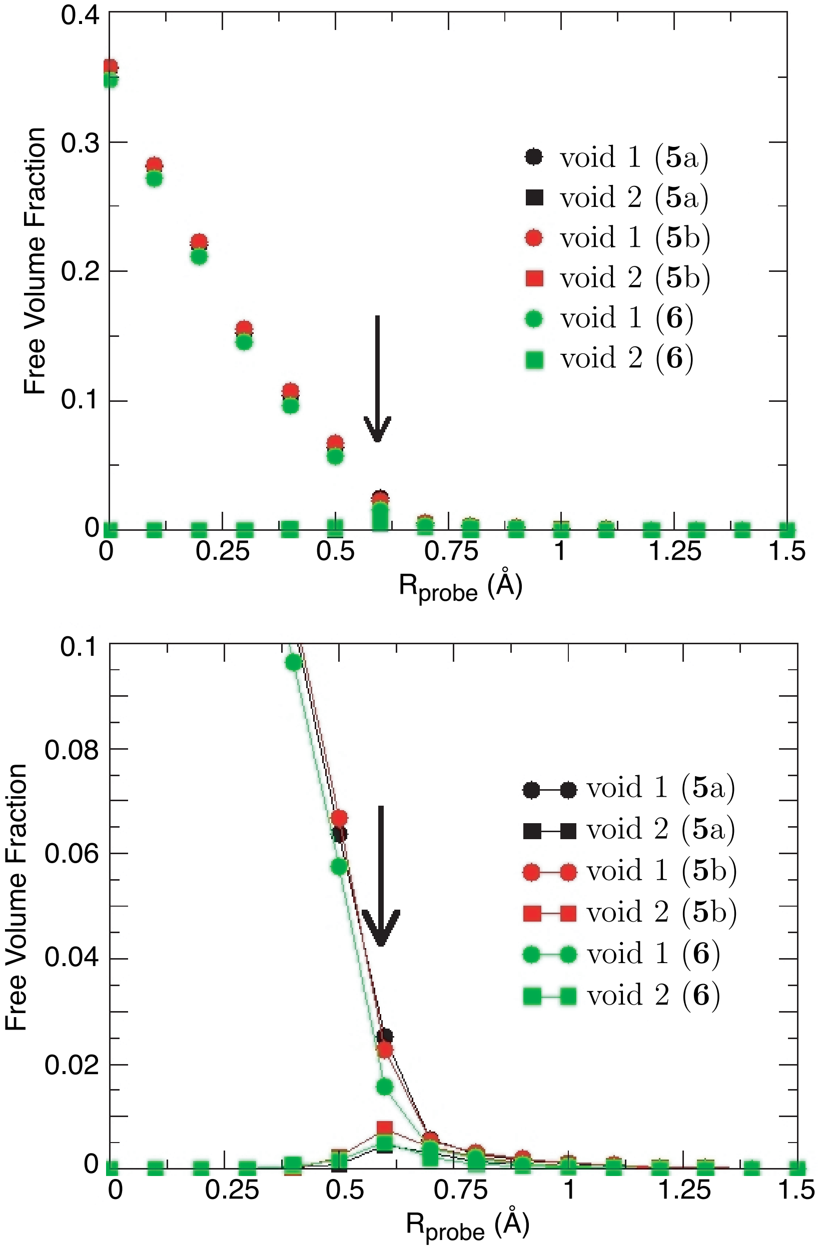

**Figure 9.5**: Comparison of void spaces in syn and anti EVOH copolymers. **5**a and **5**b are two separate samples of the syn diol polymer.

The low FV fractions for $R_p$ comparable to the size of oxygen (see Figure 9.6) in these polymers may be related to the exceptional $O_2$ barrier properties exhibited by **5**.[20–22] As a result of these simulations, comparable or even better barrier properties for **6** based on its lower FV percentage are anticipated (Figure 9.6). Moreover, polymer **6** displays a $T_g$ well above ambient temperatures.

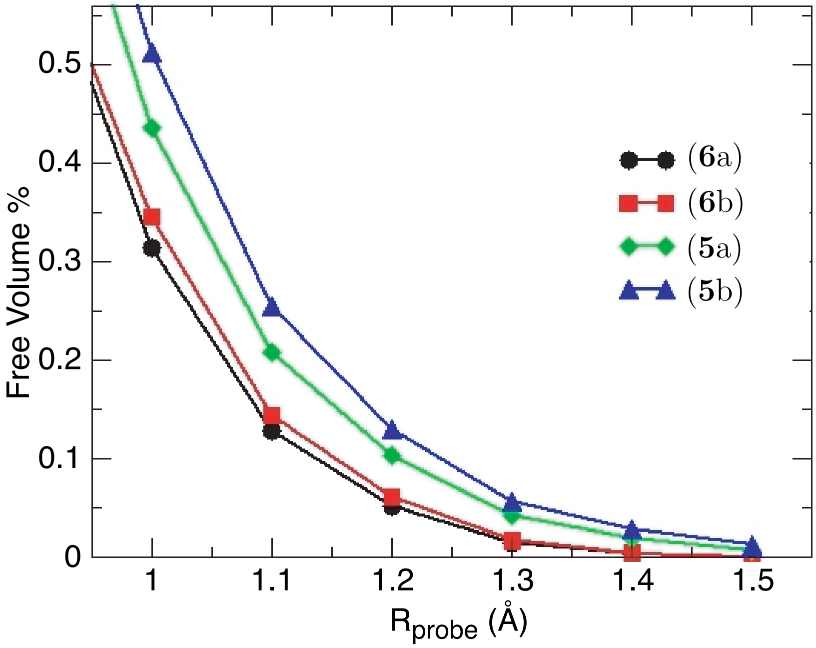

**Figure 9.6**: Comparison of void spaces in syn and anti EVOH copolymers. **6**a and **6**b and **5**a and **5**b are two separate samples of the anti and syn diol polymers, respectively.

At 300 K the hydroxyl groups are able to fluctuate over distance comparable to the size of $O_2$ (Figure 9.1). This implied that the voids in the systems evolve and suggested an exploration of the void dynamics. A significant restructuring of the FV voids on the nanosecond scale for both polymers at 300 K is observed. This is shown for polymer **5** in Figure 9.7 and for polymer **6** in Figure 9.8. Furthermore, the voids are small and well-dispersed throughout the cell consistent with the good packing in both systems.

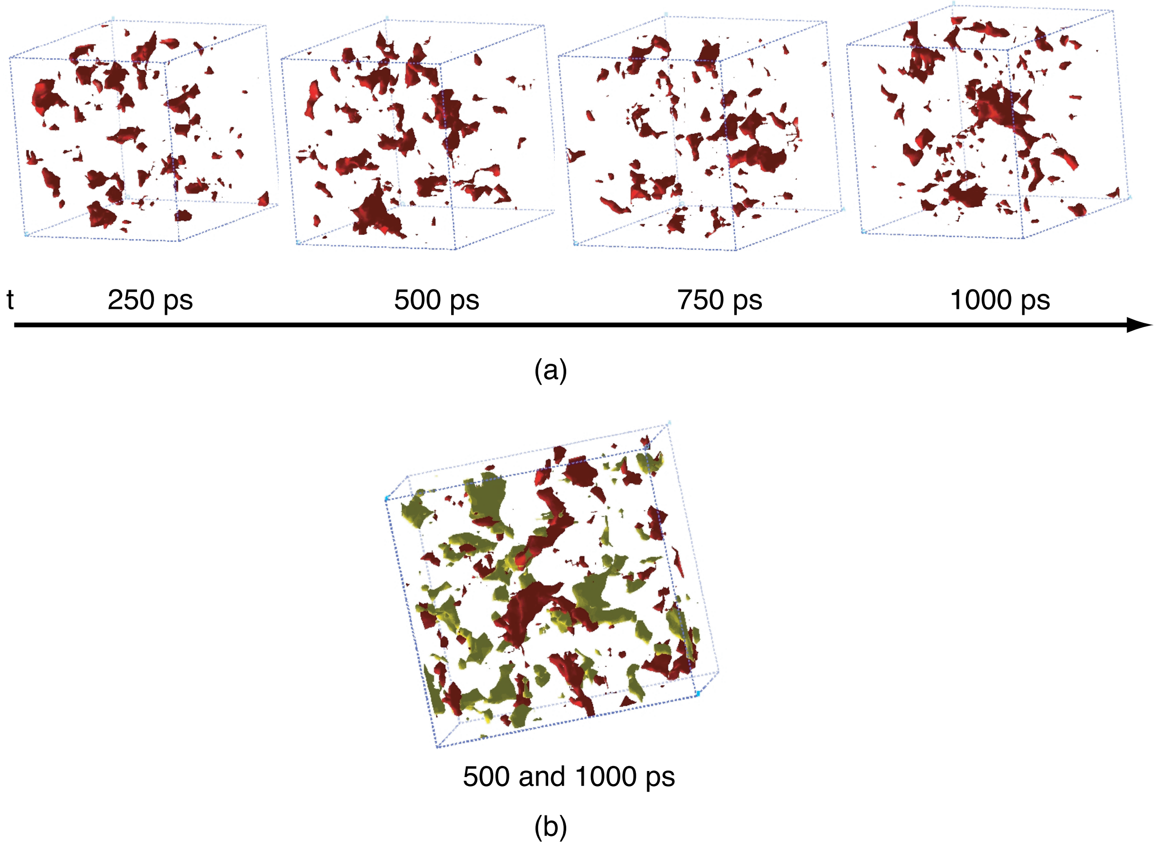

**Figure 9.7**: (a) Time evolution of the free volume for EVOH copolymer **5** in a 1 ns dynamics simulation at 300 K with a 1 Å probe radius. (b) An overlay of the free volumes at 500 and 1000 ps, indicating that different void spaces are created throughout the dynamics simulation.

### 9.4.3 Oxygen Diffusivity

In an attempt to determine the mobility of oxygen molecules in the EVOH polymers, molecular oxygen in the equilibrated structure for **5** and **6** was loaded at 300 K. The molecules were inserted at constant pressure using the sorption module of Cerius2 that implements a Grand Canonical Monte Carlo method. Based on standard solubilities of $O_2$ in organic polymers, *zero* oxygen molecules should be found in the cells (cell dimension is approximately 26 Å). To improve the collection of mobility data, an extremely high concentration of five $O_2$ molecules in both polymer systems was imposed. The pressures required to impregnate 5 oxygens were significantly higher for **6** than for **5** in agreement with the lower FV of **6**. The resultant mobilities averaged

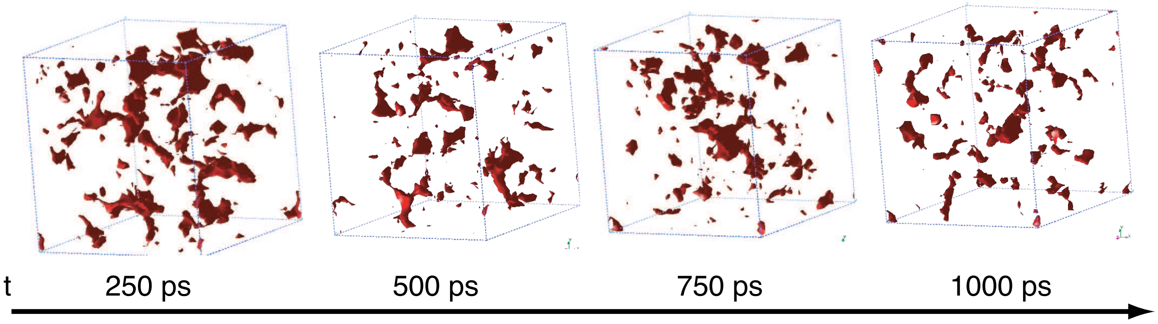

**Figure 9.8**: Time evolution of the free volume for EVOH copolymer **6** in a 1 ns dynamics simulation at 300 K with a 1 Å probe radius.

over a trajectory of 5 ns are displayed in Figure 9.9 for polymer **5** at 300 K. Note, the increased mobilities of the polymer (C and O) with respect to those observed in Figure 9.1 at the same temperature. The higher polymer mobility in the presence of oxygen indicates a plasticizing effect of this high $O_2$ concentration. Similar results have been observed previously with experiments of high pressures of Xe in polystyrene blends.[23] This is not surprising with the high loading of $O_2$ and the proximity to the expected $T_g$ (experimentally determined) for **5**.

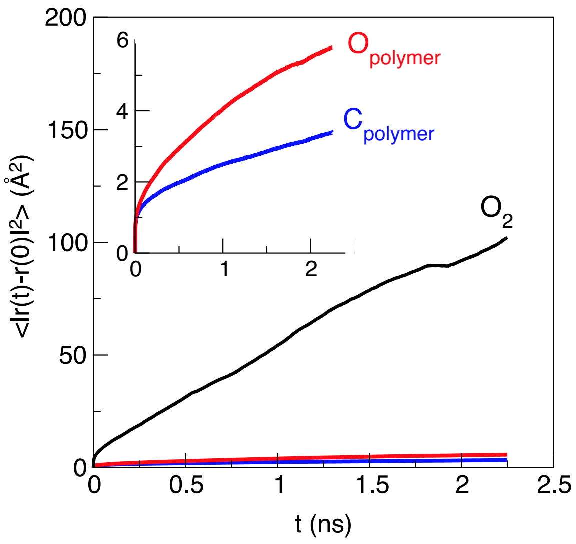

**Figure 9.9**: Average displacement of atoms in polymer and $O_2$ in molecular dynamics run.

## 9.5 Conclusions

The microscopic structure of both EVOH copolymers has been characterized in terms of hydrogen bond and FV networks. The FV is very low compared to other polymers indicating a good packing for both syn and anti diol polymers. The equilibrium densities for both polymers at 300 K were comparable (1.03 g/cm$^3$ ± 0.02 g/cm$^3$) and in good agreement with an experimental value of 1.09 g/cm$^3$. Though small, the FV voids are still mobile at 300 K in due to the hydroxyl group fluctuations. No significant differences for the mobility between the two EVOH copolymesr at 300 K was found. A striking difference in the hydrogen bond clustering was observed for these polymers. While the anti diol polymer does not form neighboring 1,2-hydrogen bonds, these features are abundant in the syn diol polymer. Perhaps more significant is the difference in extension of the hydrogen bond networks. Polymer **6** displays many short H-bond threads while **5** displays a broader distribution of cluster length with a high proportion of clusters that span over lengths comparable to the simulations cell. The extended H-bond array of polymer **5** does not, however, follow along the periphery of a single polymer chain.

# References Cited

[1] Lagaron, J. M.; Powell, A. K.; Bonner, G. *Polym. Testing* **2001,** *20,* 569–577.

[2] Lopez-Rubio, A.; Lagaron, J. M.; Gimenez, E.; Cava, D.; Hernandez-Munoz, P.; Yamamoto, T.; Gavara, R. *Macromolecules* **2003,** *36,* 9467–9476.

[3] Ramakrishnan, S. *Macromolecules* **1991,** *24,* 3753–3759.

[4] Scherman, O. A.; Kim, H. M.; Grubbs, R. H. *Macromolecules* **2002,** *35,* 5366–5371.

[5] Chapter 8 of this thesis.

[6] Accelrys Inc. *Cerius2 Modeling Environment, Release 4.0;* Accelrys Inc.: San Diego, 1999.

[7] Nose, S.; Klein, M. L. J. *Chem. Phys.* **1983,** *78,* 6928–6939.

[8] Nose, S. *J. Chem. Phys.* **1984,** *81,* 511–519.

[9] Nose, S. *Mol. Phys.* **1984,** *52,* 255–268.

[10] Nose, S. *Mol. Phys.* **1986,** *57,* 187–191.

[11] Plimpton, S. J. *J. Comp. Phys.* **1995,** *117,* 1.

[12] Plimpton, S. J.; Pollock, R.; Stevens, M. In the Eighth SIAM Conference on Parallel Processing for Scientific Computing, Minneapolis, 1997.

[13] Verlet, L. *Phys. Rev.* **1967,** *159,* 98.

[14] Hockney, R. W.; Eastwood, J. W. *Computer simulation using particles;* McGraw-Hill International Book Co.: New York, 1981.

[15] Jorgensen, W. L.; Maxwell, D. S.; Tirado-Rives, J. *J. Am. Chem. Soc.* **1996,** *118,* 11225–11236.

[16] Marrink, S. J.; Berendsen, H. J. C. *J. Phys. Chem.* **1996,** *100,* 16729–16738.

[17] Fischer, J.; Lago, S. *J. Chem. Phys.* **1983,** *78,* 5750–5758.

[18] Miyano, Y. *Fluid Phase Equilib.* **1999,** *158–160,* 29–35.

[19] Greenfield, M. L.; Theodorou, D. N. *Macromolecules* **1993,** *26,* 5461–5472.

[20] Banslaben, D. A.; Huynh-Tran, T. C.; Blanski, R. L.; Hughes, P. A.; Roberts, W. P.; Grubbs, R. H.; Hatfield, G. R. Regio-Regular Functionalized Polymeric Packaging Material. US Patent 6,203,923, March 20, 2001.

[21] Banslaben, D. A.; Huynh-Tran, T. C. T.; Blanski, R. L.; Hughes, P. A.; Roberts, W. P.; Grubbs, R. H.; Hatfield, G. R. Regio-Regular Copolymer and Methods of Forming Same. US Patent 6,506,860, January 14, 2003.

[22] Banslaben, D. A.; Huynh-Tran, T. C. T.; Blanski, R. L.; Hughes, P. A.; Roberts, W. P.; Grubbs, R. H.; Hatfield, G. R. Regio-Regular Copolymer and Methods of Forming Same. US Patent 6,153,714, November 28, 2000.

[23] Miyoshi, T.; Takegoshi, K. Terao, T. *Macromolecules* **2002,** *35,* 151–154.